Supplementary Information

Carbon nano-onion-mediated dual targeting of P-selectin and P-glycoprotein to overcome cancer drug resistance

Hai Wang[1,2,3#]*, Yutong Liang[1#], Yue Yin[2#], Jie Zhang[2], Wen Su[2], Alisa M. White[1], Bin Jiang[1], Jiangsheng Xu[1], Yuntian Zhang[1], Samantha Stewart[1], Xiongbin Lu[4], Xiaoming He[1,5,6]*

[1]Fischell Department of Bioengineering, University of Maryland, College Park, Maryland 20742, USA

[2]CAS Key Laboratory for Biomedical Effects of Nanomaterials & Nanosafety, CAS Center for Excellence in Nanoscience, National Center for Nanoscience and Technology, Beijing, 100190, China

[3]University of Chinese Academy of Sciences, Beijing, 100049, China

[4]Department of Medical and Molecular Genetics and Melvin and Bren Simon Cancer Center, Indiana University School of Medicine, Indianapolis, Indiana 46202, USA

[5]Marlene and Stewart Greenebaum Comprehensive Cancer Center, University of Maryland, Baltimore, MD 21201, USA

[6]Robert E. Fischell Institute for Biomedical Devices, University of Maryland, College Park, Maryland 20742, USA

*Correspondence should be addressed to:
wanghai@nanoctr.cn or shawnhe@umd.edu

SUPPLEMENTARY FIGURES

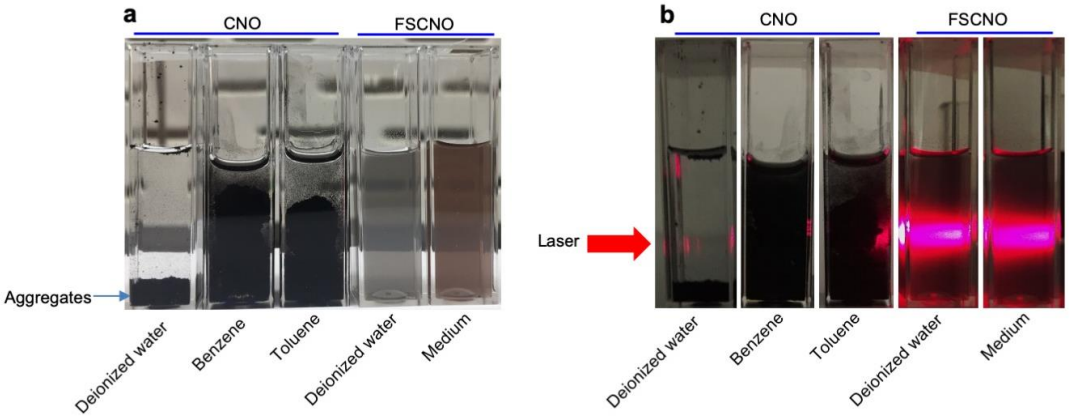

Supplementary Figure 1. Carbon nano-onions (CNOs) have poor solubility in both deionized water and organic solvent (benzene and toluene) while FSCNO nanoparticles can be stably dispersed in deionized water and medium. (**a**) A typical photograph of CNOs in deionized water, benzene and toluene (1 mg ml^{-1}) and FSCNO nanoparticles in deionized water and cell culture medium (1 mg ml^{-1}). The FSCNO nanoparticles can be well dispersed in deionized water or cell culture medium while CNOs form aggregates and sink down at the bottom of the cuvette. (**b**) A typical photograph of aforementioned solutions after shining a red laser beam (arrow) through them in dark. The light track can only be observed in FSCNO nanoparticles as a result of the Tyndall effect (i.e., scattering of laser beam by nanoparticles in solution).

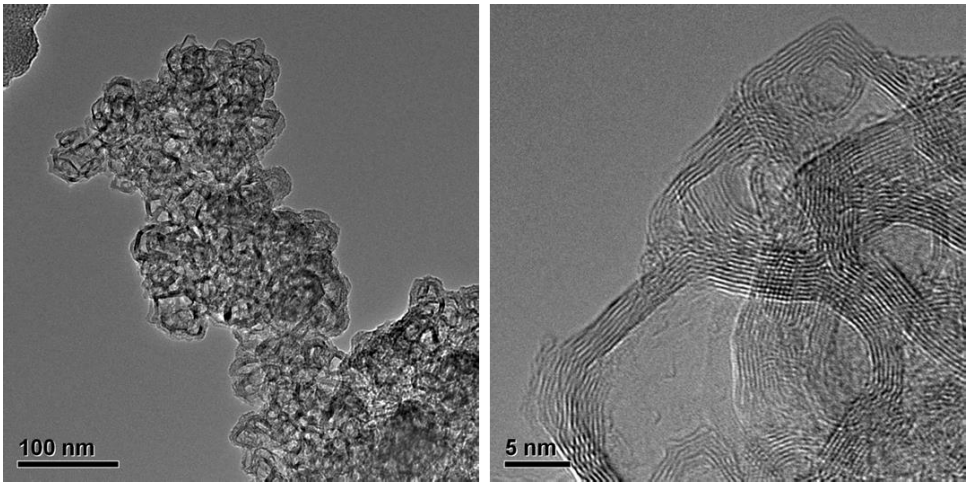

Supplementary Figure 2. High-resolution TEM images of carbon nano-onions (CNOs). The onion-like multi-layered structure is observable, particularly in the high-magnification image on the right.

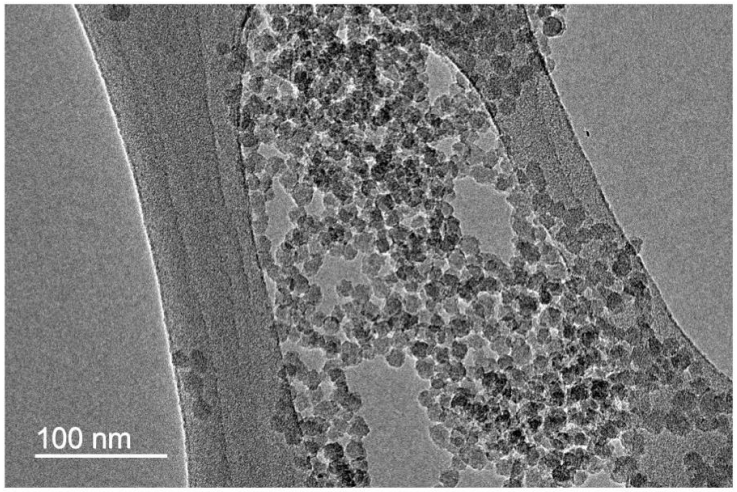

Supplementary Figure 3. TEM image of SCNO nanoparticles. The SCNO nanoparticles are smaller in size and have more homogeneous size distribution than CNOs shown in Fig. 2b.

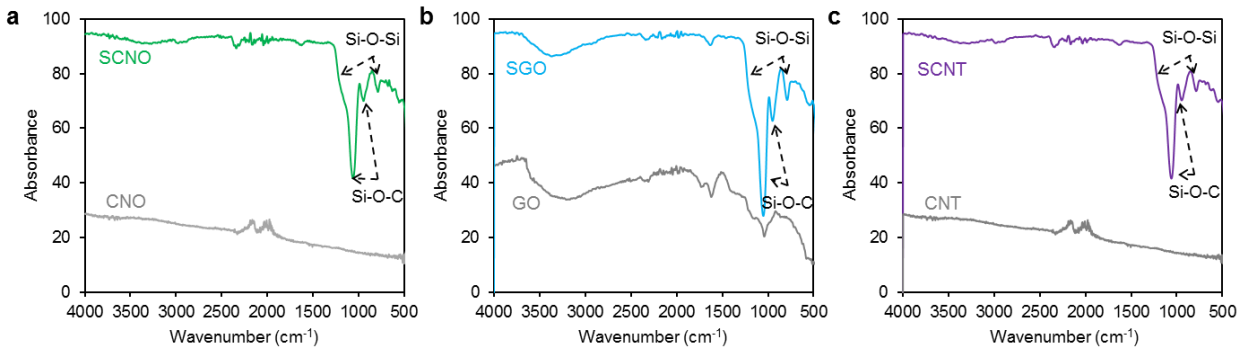

Supplementary Figure 4. FTIR spectra showing successful synthesis of the SCNO, SGO and SCNT nanoparticles. (**a**) The Fourier transform infrared (FTIR) spectra of CNO and SCNO nanoparticles showing the presence of silica (indicated by the Si-O-Si bond at 800 and 1080-1200 cm^{-1}) and the reaction between silica and CNO (indicated by the Si-O-C bond at 954 and 1070 cm^{-1}) according to the literature (Jeong et al. Angew. Chem. Int. Ed. 2009, 48, 5296-5299). (**b**-**c**) FTIR spectra of GO and SGO (**b**) and CNT and SCNT (**c**) showing the presence of silica and the reaction between silica and GO/CNT with similar peaks shown in (a) for SCNO.

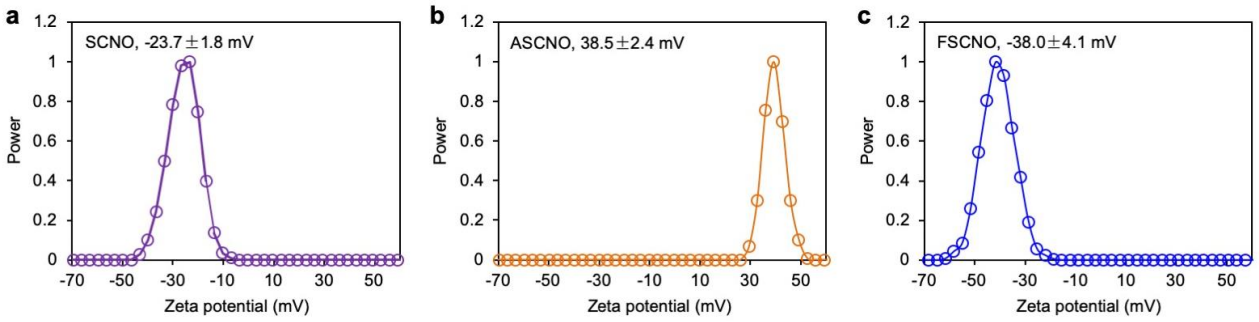

Supplementary Figure 5. Surface zeta potential of SCNO, ASCNO, and FSCNO nanoparticles in deionized water. (**a**) The surface zeta potential of SCNO nanoparticles is negative. (**b**) It becomes positive after coating them with APTMS to form the ASCNO nanoparticles. (**c**) The zeta potential returns to negative after incubating the ASCNO nanoparticles with fucoidan, indicating successful decoration of fucoidan to form the FSCNO nanoparticles.

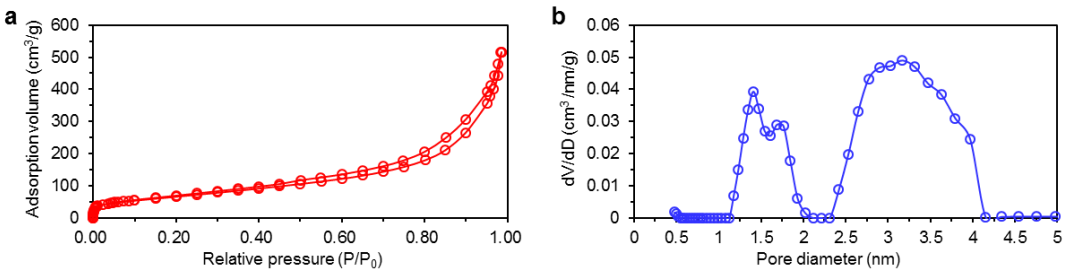

Supplementary Figure 6. Nitrogen gas sorption measurements of FSCNO nanoparticles. (**a**) Nitrogen gas adsorption-desorption isotherms of the FSCNO nanoparticles. (**b**) pore size distribution within the FSCNO nanoparticles.

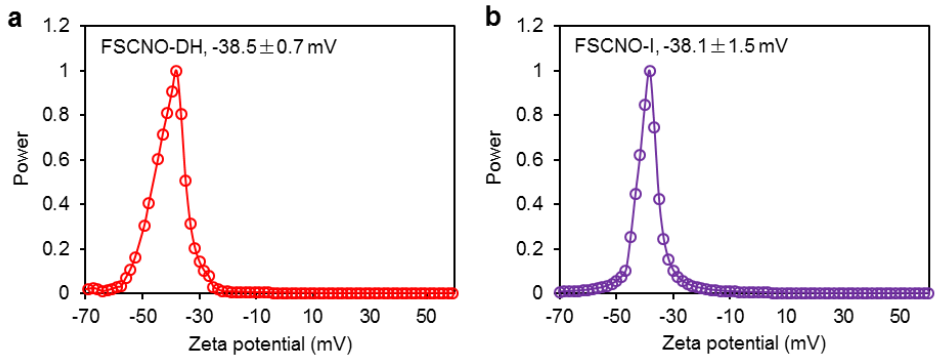

Supplementary Figure 7. Surface zeta potential agent-laden nanoparticles in deionized water. (**a**) FSCNO-DH nanoparticles loaded with DOX and HM. (**b**) FSCNO-I nanoparticles loaded with ICG. The zeta potential of therapeutic agents laden-FSCNO nanoparticles (**Supplementary Figure 5c**) is similar to that of FSCNO nanoparticles without any therapeutic agent, suggesting the drugs are not located on the surface of FSCNO nanoparticles.

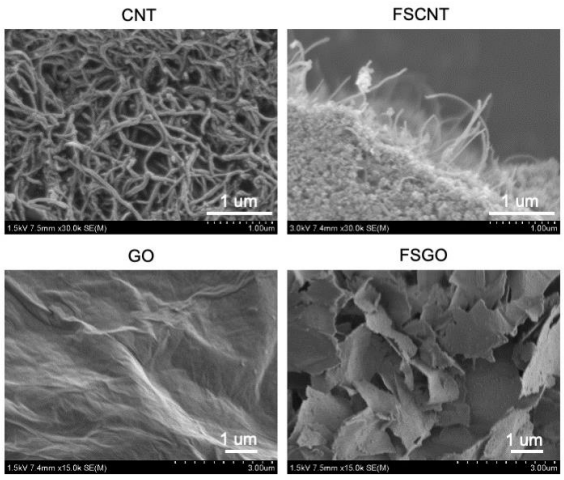

Supplementary Figure 8. SEM images of carbon nanotubes (CNT), graphene oxides (GOs), FSCNT nanoparticles, and FSGO nanoparticles. The morphology of CNTs and FSCNT are different although they all have the tubular morphology. Similarly, the FSGO nanoparticles are thicker than the GOs although they all have the laminar morphology.

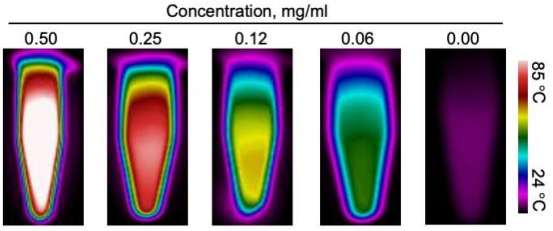

Supplementary Figure 9. Photothermal effect of FSCNO nanoparticles. Near infrared thermographs of the aqueous solutions of FSCNO nanoparticles in tube at different concentrations (0.00, 0.06, 0.12, 0.25, and 0.50 mg ml^{-1}) in centrifuge tube after irradiation with NIR laser (1.0 W cm^{-2}) for 2 min.

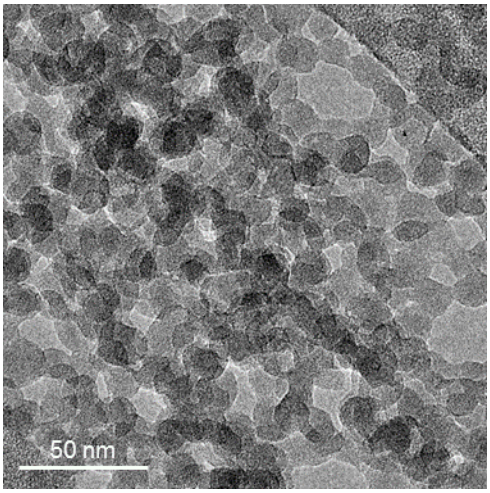

Supplementary Figure 10. TEM image of FSCNO nanoparticles after NIR laser irradiation. The image shows no evident damage to the integrity of the nanoparticles after the laser irradiation.

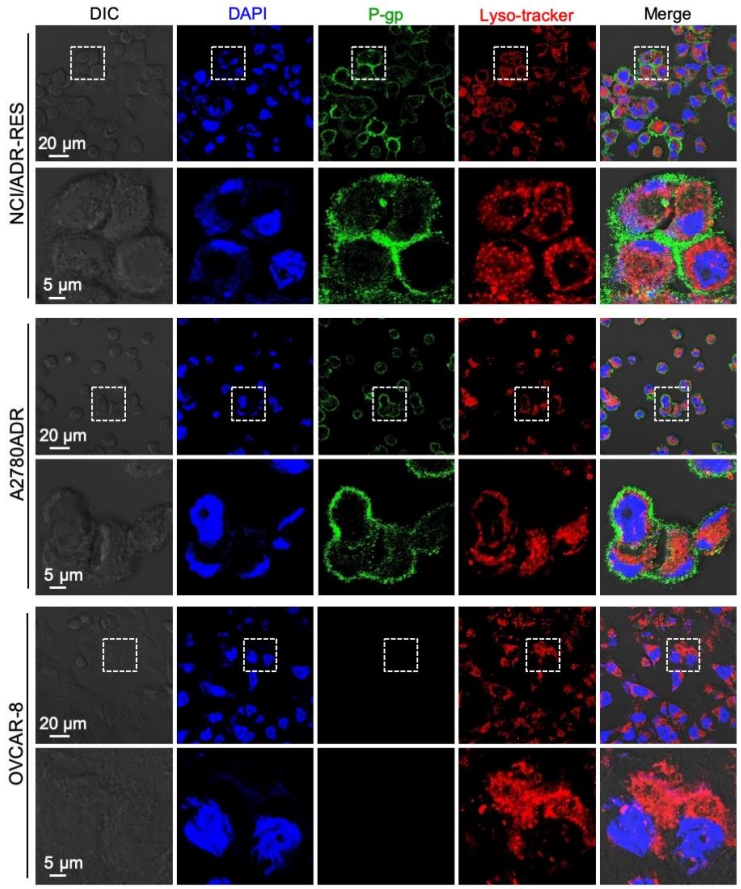

Supplementary Figure 11. Expression of P-gp in NCI/ADR-RES, A2780ADR, and OVCAR-8 cells. The confocal images show the expression of P-gp in both the NCI/ADR-RES and A2780ADR multidrug-resistant cancer cells but not the non-drug resistant OVCAR-8 cells.

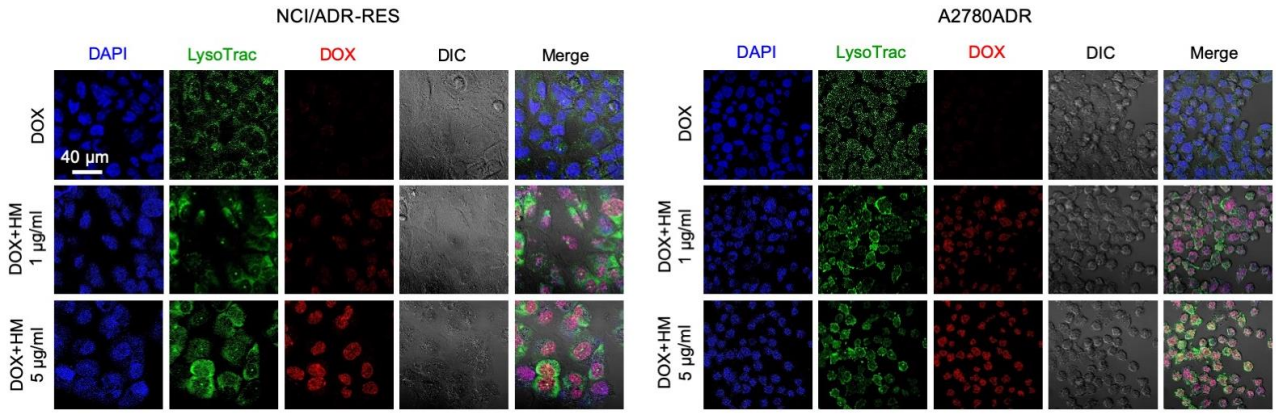

Supplementary Figure 12. Overcoming drug resistance of NCI/ADR-RES and A2780ADR cells with P-gp inhibitor. Fluorescence images of DOX show the drug resistant property of NCI/ADR-RES and A2780ADR cells. However, DOX can enter the cells if they are co-treated with HM (1 or 5 μg ml^{-1}), suggesting co-treatment of DOX and P-gp inhibitor is a feasible way to overcome the multidrug resistance of the cancer cells.

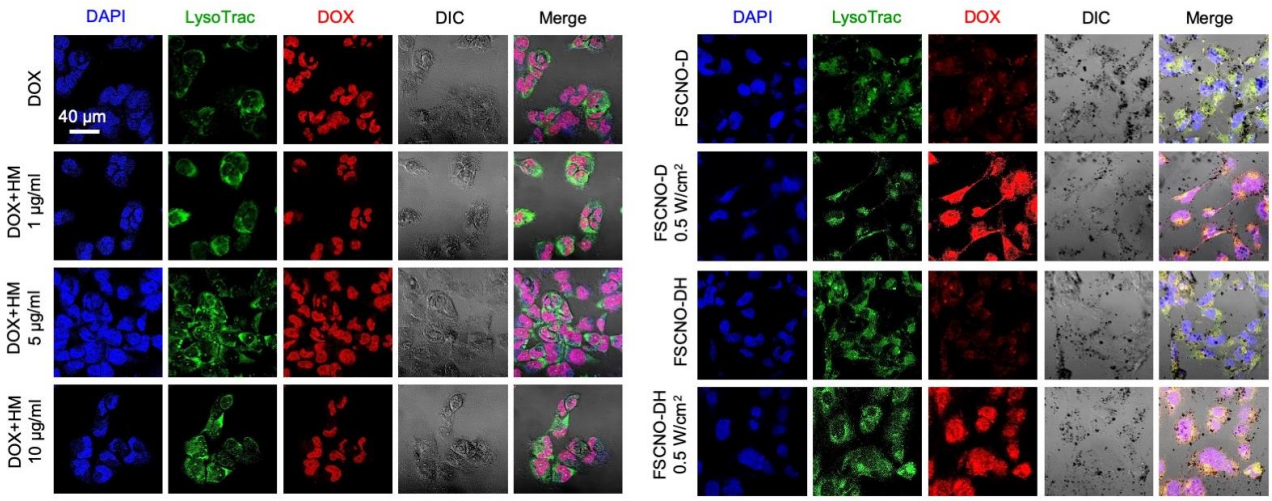

Supplementary Figure 13. Minimal effect of P-gp inhibitor on the uptake of DOX by OVCAR-8 cells. Fluorescence images of DOX show P-gp inhibitor does not change the intensity of free DOX in OVCAR-8 cells. Similarly, there is no obvious difference between the OVCAR-8 cells treated with FSCNO-D and FSCNO-DH nanoparticles, either without or with NIR laser irradiation (0.5 W cm^{-2} for 1 min). Of note, the fluorescence intensity of DOX in cells treated with FSCNO-D or FSCNO-DH nanoparticles is enhanced if the cells are also treated with NIR laser irradiation, which might be due to the self-quenching effect of DOX inside nanoparticles as shown in Fig. 2g.

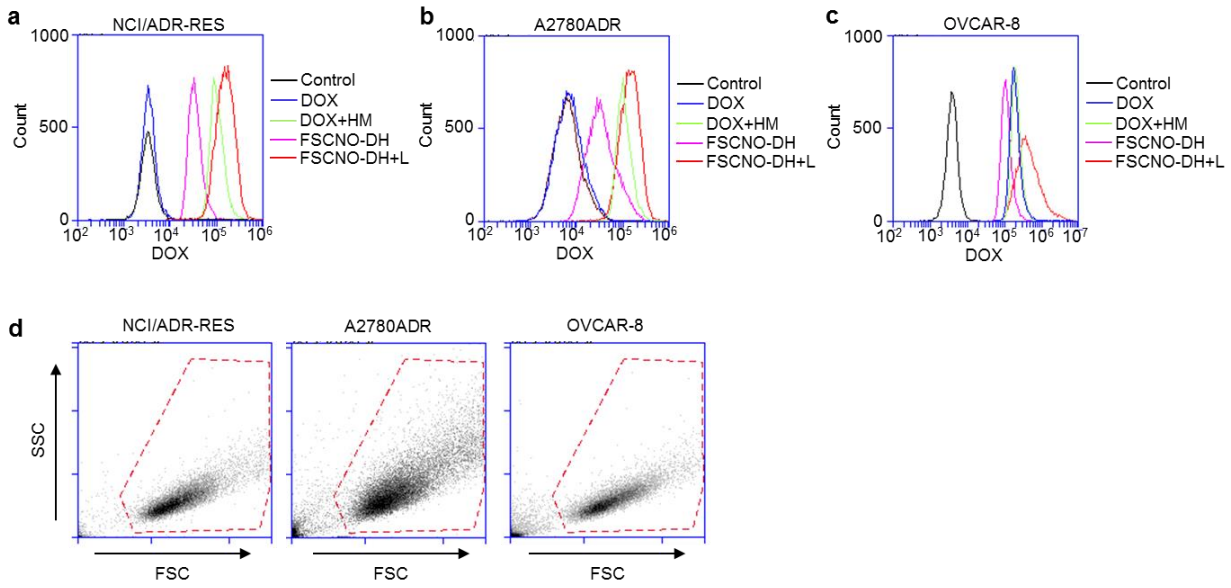

Supplementary Figure 14. Flow cytometry analyses of DOX in NCI/ADR-RES, A2780ADR, and OVCAR-8 cells after various treatments. (**a**-**b**) The data indicate that DOX in NCI/ADR-RES (**a**) and A2780ADR (**b**) cells is minimal after treated with free DOX, but can be greatly increased if the free DOX is combined with HM (DOX+HM) for treating the cells. The fluorescence intensity in cells treated with FSCNO-DH+L is stronger than that for the FSCNO-DH treatment, probably due to the self-quenching effect of DOX fluorescence in the FSCNO nanoparticles (Fig. 2g). (**c**) HM has minimal effect on the cellular uptake of DOX in OVCAR-8 cells. (**d**) Gating strategy used for the flow cytometry analyses. All the cells were selected except for the debris.

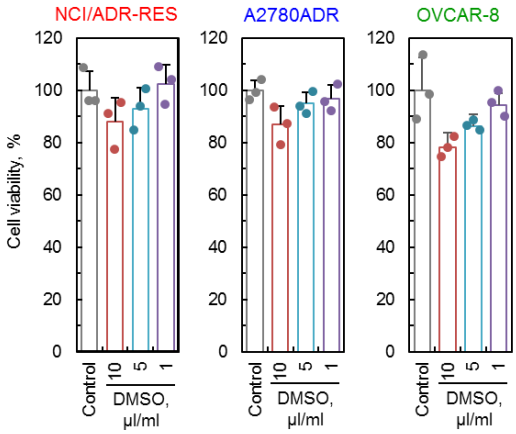

Supplementary Figure 15. Toxicity of DMSO to cancer cells. DMSO was used to dissolve HM in cell culture media for cell viability studies with the viability being shown in Fig. 4d. DMSO at concentrations of 5 and 10 µl ml^{-1} are slightly toxic to all the three different kinds of cells. Error bars represent ± s.d. (n = 3 independent replicates).

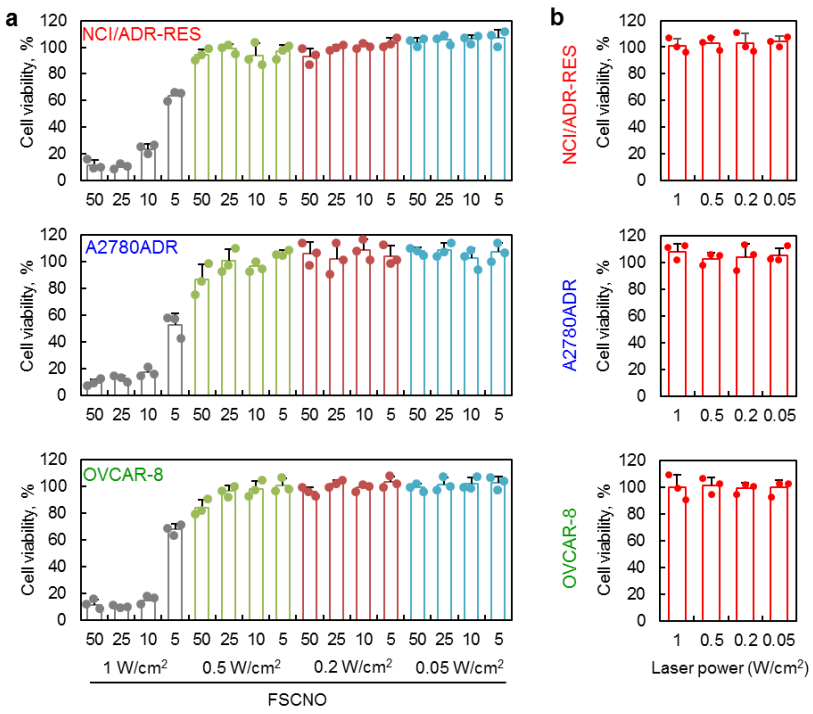

Supplementary Figure 16. The nontoxic nature of empty FSCNO nanoparticles. (**a**) Cell viability of NCI/ADR-RES, A2780ADR, and OVCAR-8 cells after treated with empty FSCNO nanoparticles and NIR laser irradiation of various powers. The data show that a laser power below 1 W cm^{-2} does not cause obvious toxicity to any of the cells. The cytotoxicity at 1 W cm^{-2} should be due to the superior photothermal effect of the empty nanoparticles. Error bars represent ± s.d. (n = 3 independent replicates). (**b**) Cell viability of NCI/ADR-RES, A2780ADR, and OVCAR-8 cells after treated with laser (1 W cm^{-2} for 2 min) alone, showing the NIR laser treatments alone does not kill the tumor cells. Error bars represent ± s.d. (n = 3 independent replicates).

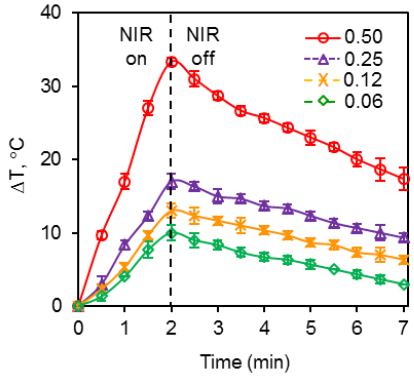

Supplementary Figure 17. Photothermal effect of FSCNO nanoparticles under laser power of 0.2 W cm^{-2}. The change in temperature in the aqueous solution of FSCNO nanoparticles (0.06, 0.12, 0.25, and 0.5 mg ml^{-1}) increases upon NIR laser irradiation (0.2 W cm^{-2}) for 2 min with the increase of the nanoparticle concentration. Error bars represent ± s.d. (n = 3 independent replicates).

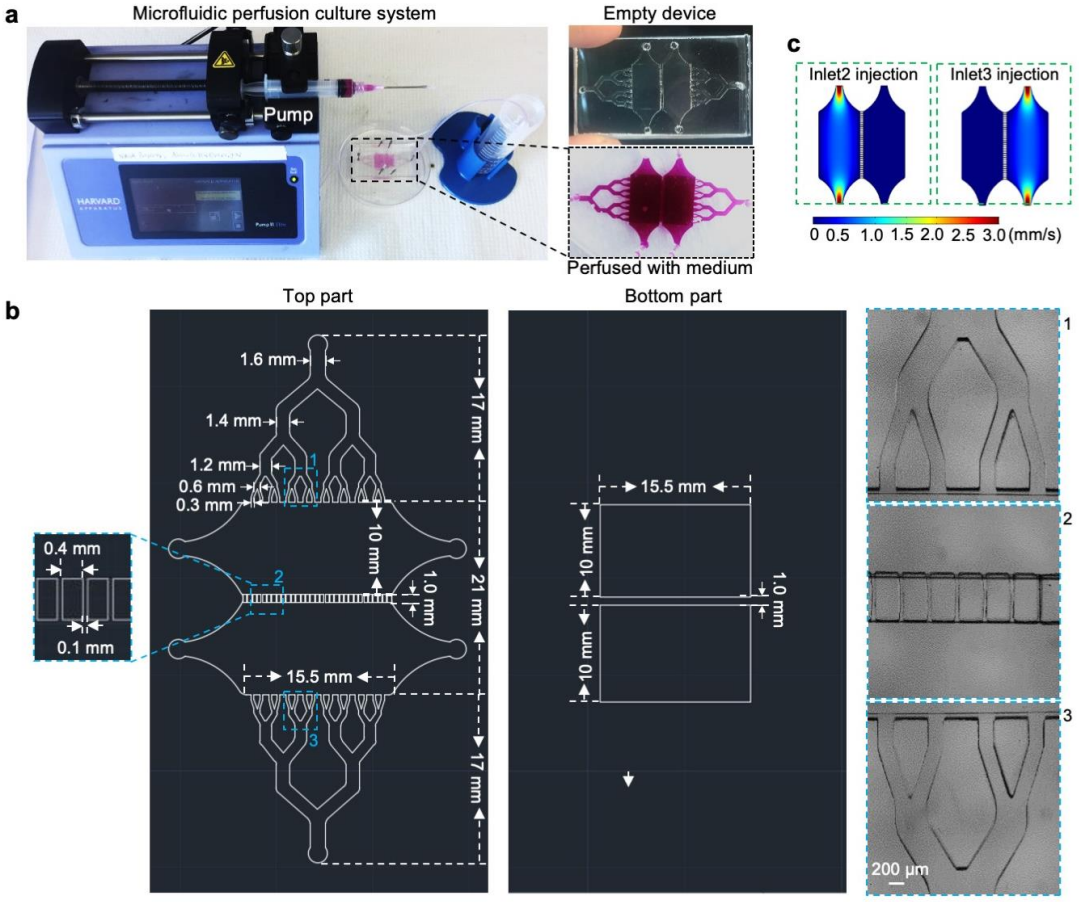

Supplementary Figure 18. Microfluidic perfusion culture system used to study the tumor vasculature-targeting effect of FSCNO nanoparticles. (**a**) Photograph of the culture system showing cell culture medium is injected into the microfluidic device using a syringe pump, and the medium flowing out the device is collected into a 50 ml centrifuge tube. (**b**) Detailed design of the top and bottom PDMS parts that are bonded together by plasma treatment. The top part contains all the microchannels for injecting cells and flowing cell culture medium. The two cell culture chambers are in the bottom part. The selected areas with zoom-in views are the entrance channels of cell culture medium (1), partition walls (made of micropillars spaced at 100 μm) between the two chambers (2), and the exit channels of cell culture medium. The height of the channels in the top part and the two chambers in the bottom part is 300 μm, respectively. (**c**) Computational modeling results of velocity distribution in the device when injecting cell suspensions from inlet2 and inlet3. The data show that cell injection via inlet2 and inlet3 is independent for each chamber, which is also what we observed during experiments.

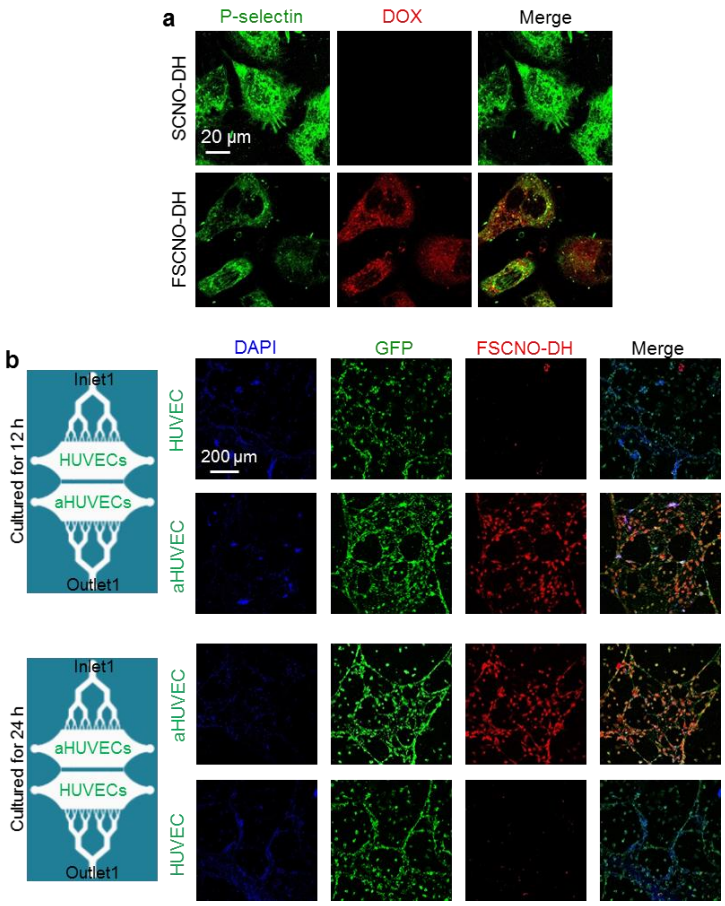

Supplementary Figure 19. P-selectin targeting capability of FSCNO nanoparticles. In order to check the stability of decoration of fucoidan on the SCNO nanoparticles, FSCNO-DH nanoparticles were incubated in cell culture medium for 2 day and then used for further experiments. (**a**) Confocal images of pre-cooled aHUVECs after incubated with SCNO-DH and FSCNO-DH nanoparticles (10 μg ml^{-1} for DOX and 5 μg ml^{-1} for HM). The cells were cooled on ice for 3 h to minimize their metabolic and uptake activities. (**b**) Schematic and confocal images of GFP expression HUVECs (in the chamber next to inlet1 or outlet1) and aHUVECs (in the chamber next to outlet1 or inlet1) cultured in the microfluidic device perfused with pure medium for 24 h and then in medium containing FSCNO-DH nanoparticles for 3 h. The data indicates that FSCNO-DH nanoparticles are stable and can target the aHUVECs efficiently after 2 days of incubation in cell culture medium.

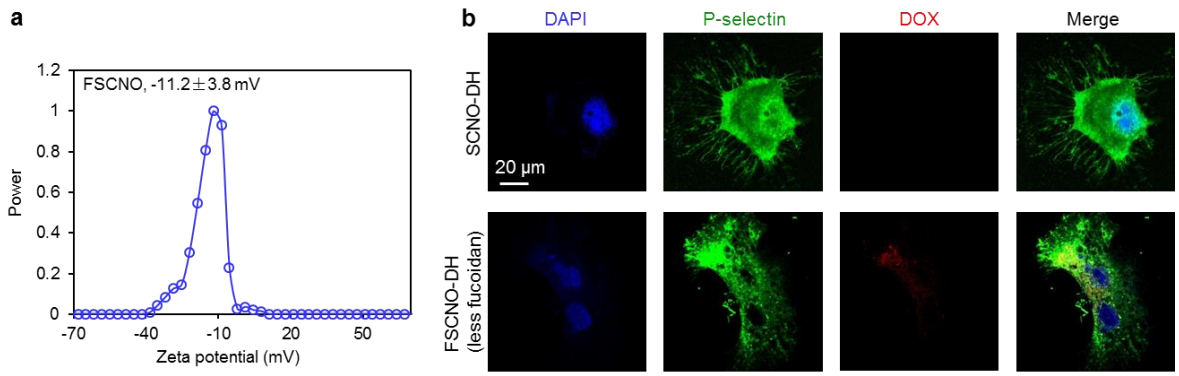

Supplementary Figure 20. The density of fucoidan can affect the targeting capability of FSCNO nanoparticles. (**a**) The surface zeta potential of F^{low}SCNO nanoparticles prepared with reduced fucoidan (2 mg ml^{-1}) is is higher than that of FSCNO nanoparticles (prepared with 2 mg ml^{-1} durig syntheis of the nanoparticles). (**b**) F^{low}SCNO-DH nanoparticles can target the aHUVECs better than the SCNO-DH nanoparticles (with no fucoidan on their surface), but they are not as efficient as the FSCNO nanoparticles (**Figure 5b** and **Supplementary Figure 19a**) for the targeting.

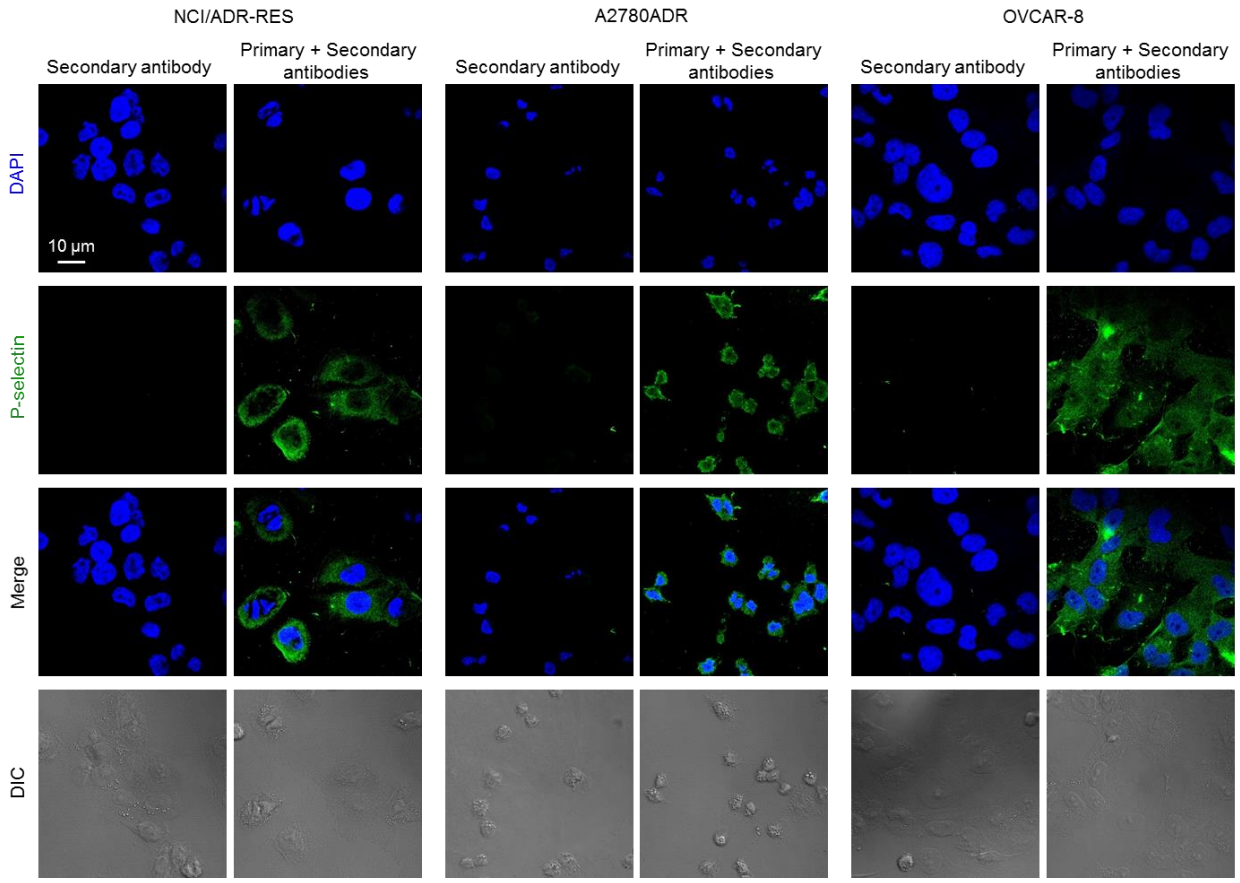

Supplementary Figure 21. Expression of P-selectin in NCI/ADR-RES, A2780ADR, and OVCAR-8 cells. Confocal images of the three types of cells after treated with either secondary antibody alone or both the P-selectin primary antibody and secondary antibody, showing P-selectin is expressed on all the three types of cancer cells.

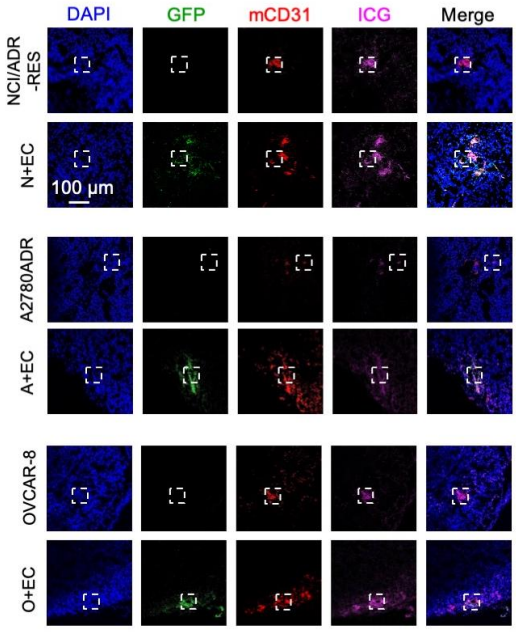

Supplementary Figure 22. Fluorescence images of ICG, GFP, and CD31 in tumors of mice treated with FSCNO-I nanoparticles. The data indicates that aHUVECs are involved in forming the tumor vasculature and FSCNO-I nanoparticles can target the tumor vasculature formed from both the endogenous host cells and the implanted exogenous aHUVECs**.** The selected areas are shown in Fig. 7e-g.

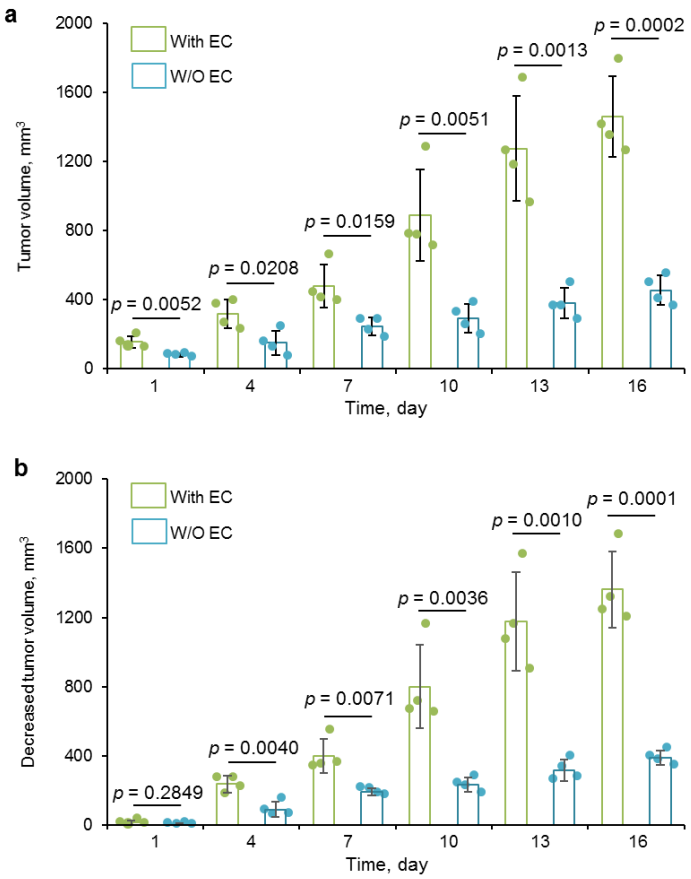

Supplementary Figure 23. Effect of co-injected aHUVECs on the growth of A2780ADR and treatment of FSCNO-DH nanoparticles with laser irradiation. (**a**) The data show that co-injection of aHUVECs and A2780ADR cells (With EC) can significantly increase the A2780ADR tumor growth compared to injection of the A2780ADR cells alone without the aHUVECs (W/O EC). (**b**) The decreased tumor volume of FSCNO-DH+L group compared with Saline group for the tumor grown with or without co-injection of aHUVECs. Error bars represent ± s.d. (n = 4 mice for each group) and statistical significance was assessed by unpaired two-sided Student *t*-test.

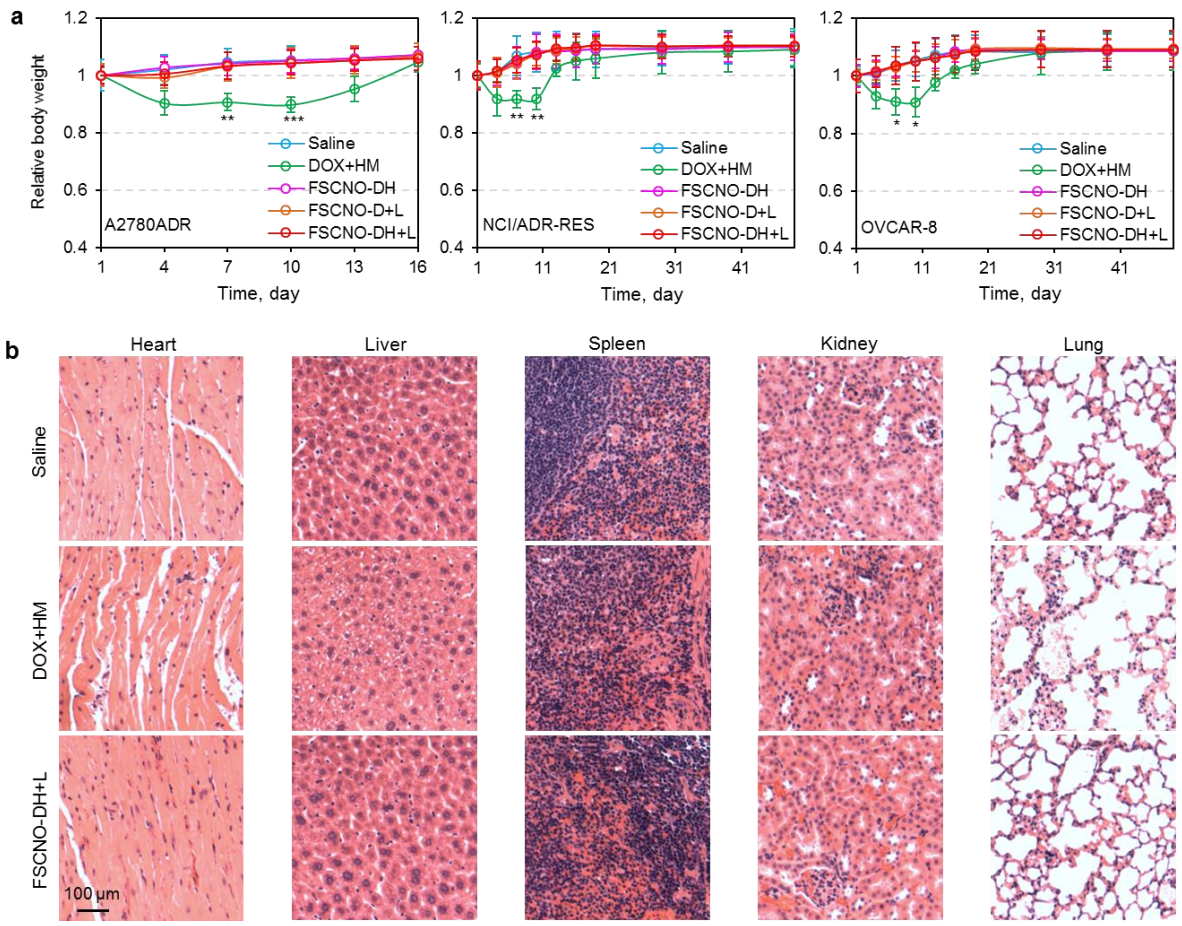

Supplementary Figure 24. No evident systemic toxicity for the treatment of FSCNO-DH nanoparticles with NIR laser irradiation. (**a**) Body weight of mice from A2780ADR, NCI/ADR-RES, and OVCAR-8 groups with the various treatments showing no significant difference between the Saline and FSCNO-DH+L group. Significant drop of the body weight was observed for the DOX+HM group, indicating free DOX and HM at the dose used in this study could cause significant side effects. (**b**) Representative hematoxylin & eosin (H&E) stained tissue of major organs in mice from A2780ADR group with the various treatments showing no significant difference between the Saline and FSCNO-DH+L treated with saline, DOX+HM, or FSCNO-DH with NIR laser irradiation (FSCNO-DH+L). The data show the DOX+HM treatment could cause evident damage to the mouse heart and liver, consistent with the significant drop in body weight of mice in the DOX+HM group. No evident damage to the major organs is observable for the FSCNO-DH+L treatment. Error bars represent ± s.d.(n = 4 mice for each group) and statistical significance was assessed by One-way ANOVA with Dunnett's post hoc analysis. $^{**}p = 0.0019$, $^{***}p = 0.0005$, $^{**}p = 0.0058$, $^{**}p = 0.0015$, $^{**}p = 0.0082$, and $^{**}p = 0.0034$ (left to right).

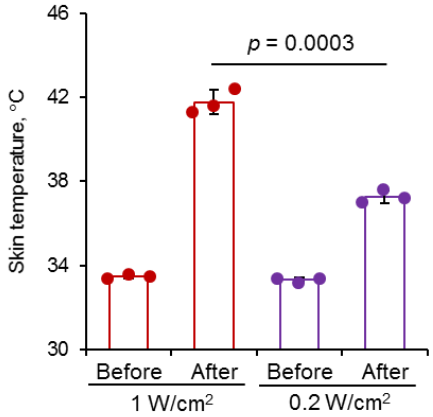

Supplementary Figure 25. Skin temperature of mice (n = 3) after irradiated with NIR laser for 1 min with power of 1 and 0.2 W cm^{-2}. The data indicate that NIR laser could increase the temperature of tissue and the importance of using a low laser power to trigger the drug release without causing significant thermal damage to the normal tissue surrounding tumor. Error bars represent ± s.d. (n = 3 independent replicates) and statistical significance was assessed by unpaired two-sided Student *t*-test.

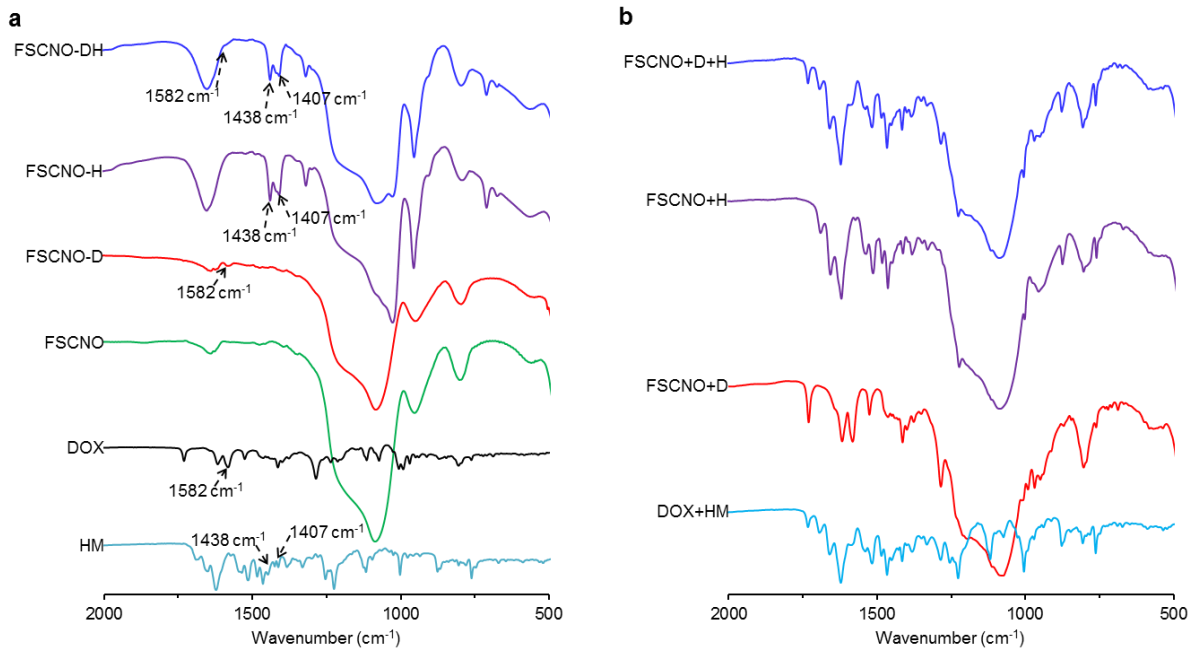

Supplementary Figure 26. FTIR spectra showing successful encapsulation of both DOX and HM in FSCNO nanoparticles. (**a**) The FTIR spectra of HM; DOX; and the FSCNO, FSCNO-D, FSCNO-H, and FSCNO-DH nanoparticles, showing the presence of DOX (indicated by the peak of aromatic bonds at 1582 cm^{-1}) in FSCNO-D and FSCNO-DH nanoparticles. The presence of HM is confirmed by the peaks of the methyl and carboxyl groups at 1438 and 1407 cm^{-1}, respectively, in HM and the FSCNO-H and FSCNO-DH nanoparticles. (**b**) FTIR spectra of the mixtures of DOX and HM (DOX+HM); DOX and FSCNO (FSCNO+D); HM and FSCNO (FSCNO+H); and DOX, HM, and FSCNO nanoparticles (FSCNO+D+H).

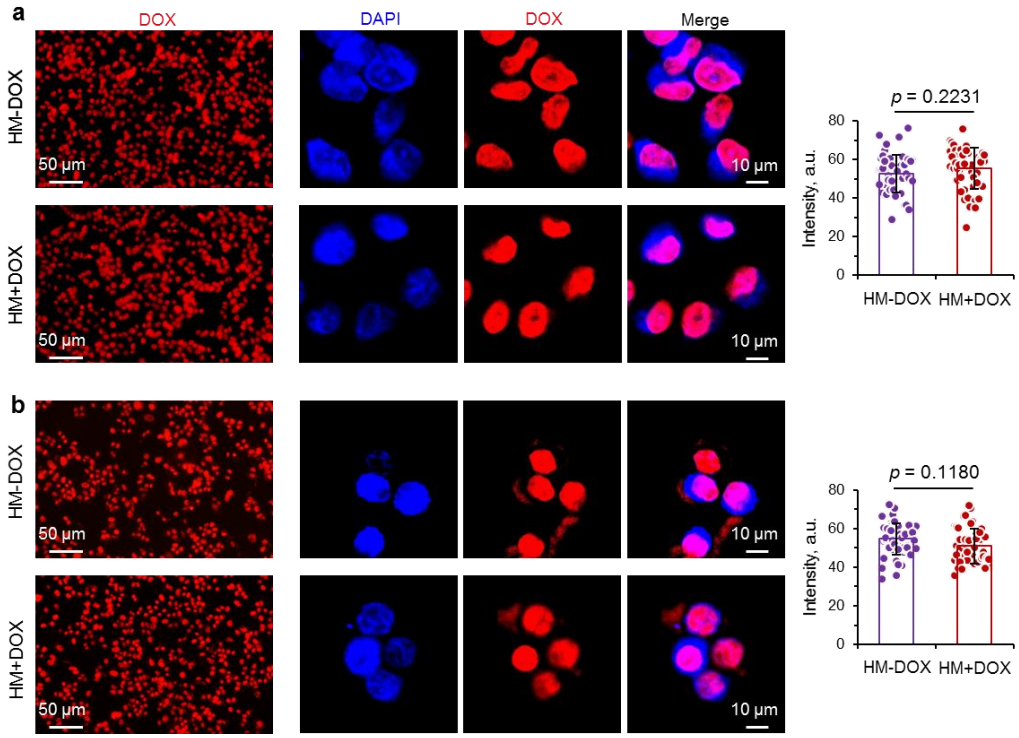

Supplementary Figure 27. Cellular uptake of DOX by drug resistant cells treated with HM-DOX and HM+DOX. The low (first column on the left) and high magnification images of (**a**) NCI/ADR-RES and (**b**) A2780ADR drug resistant cells treated with HM-DOX (pre-treated with HM for 30 min before incubation with HM and DOX for 3 h) or HM+DOX (no pre-treatment with HM before incubation with HM and DOX for 3 h). The DOX and HM concentrations are 10 and 5 μg ml^{-1}, respectively, for all the experiments. The fluorescence intensity of DOX in cells are calculated by the NIH ImageJ software. Error bars represent ± s.d. (n = 50 cells over 3 independent replicates) and statistical significance was assessed by unpaired two-sided Student *t*-test. No adjustments were made for multiple comparisons.

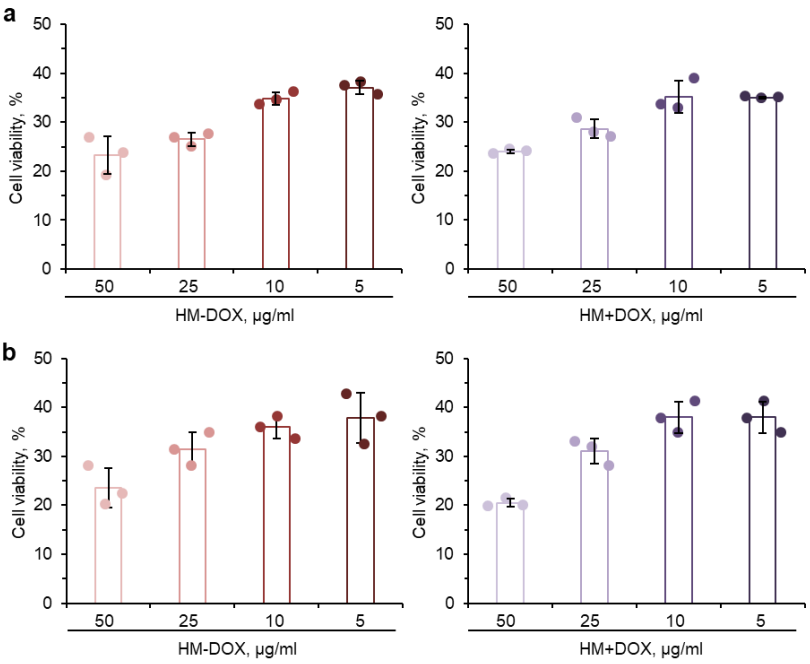

Supplementary Figure 28. Cytotoxicity of HM-DOX and HM+DOX treatments on drug resistant cells. Cell viability of (**a**) NCI/ADR-RES and (**b**) A2780ADR drug resistant cells treated with HM-DOX (pre-treated with HM for 30 min before incubation with HM and DOX) or HM+DOX (no pre-treatment with HM before incubation with HM and DOX) for 24h. The HM concentration is 5 µg ml^{-1}. There is no significant difference in cell viability between the HM-DOX and HM+DOX treatments under the same concentrations of DOX for both the NCI/ADR-RES and A2780ADR cells. Error bars represent ± s.d. (n = 3 independent replicates).